NASA CONTRACTOR REPORT

NASA CR-2138

NASA CR-2138

FINITE-AMPLITUDE PRESSURE WAVES IN THE RADIAL MODE OF A CYLINDER

by Isoroku Kubo and Franklin K. Moore

Prepared by
CORNELL UNIVERSITY
Ithaca, N.Y. 14850
for Lewis Research Center

NATIONAL AERONAUTICS AND SPACE ADMINISTRATION • WASHINGTON, D. C. • NOVEMBER 1972

1. Report No.	2. Government Accession No.	3. Recipient's Catalog No.
CR-2138		

4. Title and Subtitle	5. Report Date
FINITE-AMPLITUDE PRESSURE WAVES IN THE RADIAL MODE OF A CYLINDER	November 1972
	6. Performing Organization Code
7. Author(s)	8. Performing Organization Report No.
Isoroku Kubo and Franklin K. Moore	None
	10. Work Unit No.
9. Performing Organization Name and Address	
Cornell University Ithaca, New York 14850	11. Contract or Grant No. NGL 33-010-042
	13. Type of Report and Period Covered
12. Sponsoring Agency Name and Address	Contractor Report
National Aeronautics and Space Administration Washington, D.C. 20546	14. Sponsoring Agency Code

15. Supplementary Notes

Project Manager, John C. Evvard, NASA Lewis Research Center, Cleveland, Ohio

16. Abstract

A numerical study of finite-strength, isentropic pressure waves transverse to the axis of a circular cylinder is made for the radial resonant mode. The waves occur in a gas otherwise at rest, filling the cylinder. A method of characteristics is used for the numerical solution. For small but finite amplitudes, calculations indicate the existence of waves of permanent potential form. For larger amplitudes, a shock is indicated to occur. The critical value of the initial amplitude parameter in the power series is found to be 0.06 to 0.08, under various types of initial conditions.

17. Key Words (Suggested by Author(s))		18. Distribution Statement
Shock wave	Finite amplitude	Unclassified - unlimited
Radial mode	Isentropic	
Cylindrical wave		

19. Security Classif. (of this report)	20. Security Classif. (of this page)	21. No. of Pages	22. Price*
Unclassified	Unclassified	35	$3.00

* For sale by the National Technical Information Service, Springfield, Virginia 22151

SUMMARY

A numerical study of finite-strength, isentropic pressure waves transverse to the axis of a circular cylinder is made for the radial resonant mode. The waves occur in a gas otherwise at rest, filling the cylinder. A method of characteristics is used for the numerical solution.

For small but finite amplitudes, calculations indicate the existence of waves of permanent potential form. For larger amplitudes, a shock is indicated to occur. The critical value of the initial amplitude parameter in the power series is found to be 0.06 to 0.08, under various types of initial conditions.

INTRODUCTION

Combustion instability involving large pressure oscillations in the combustion chambers of rocket and jet engines has been observed. In (1), (2) and (3), these oscillations were analyzed on the assumption that oscillations were so weak that the classical acoustic theory is valid. However, a propagating plane wave of finite strength will eventually develop into a shock. Thus, one might expect that the high observed pressures imply the presence of shocks. Actually, in a cylindrical case, a shock may possibly fail to appear owing to the wave-scattering effect of the chamber wall. Moore and Maslen [4] studied finite transverse waves in a circular cylinder, assuming that the disturbance velocity potential could be expanded in a power series in amplitude. They found solutions for the first three approximations to be periodic in time, whereas only the first approximation is purely periodic in the plane-wave case. They concluded that finite-strength, shock-free oscillations in a cylinder were possible for some range of amplitude.

The present study employs numerical solutions of the dynamic equations to find a critical value of the amplitude, up to which the power series converges for the radial cylindrical mode, and there exists a permanent strong transverse oscillation without a shock.

FORMULATION OF THE PROBLEM

Differential Equations

An isentropic, irrotational fluid motion is governed by the following equations:

Continuity
$$\rho_t + \nabla \cdot (\rho \underline{q}) = 0 \tag{1a}$$

Momentum
$$\phi_t + \frac{q^2}{2} + \frac{1}{\gamma-1}\frac{p}{\rho} = \frac{\bar{a}^2}{\gamma-1} \tag{1b}$$

State isentropy
$$p \propto \rho^{\gamma} \tag{1c}$$

Velocity potential
$$\underline{q} \equiv \nabla\phi \tag{1d}$$

where $\bar{a}$ is the speed of sound in the absence of any oscillation. By eliminating p, ρ and $\underline{q}$ from eqs. (1), the following equation for velocity potential is obtained:

$$\phi_{tt} - \{\bar{a}^2 - (\gamma - 1)(\phi_t + \frac{1}{2}\phi_r^2 + \frac{1}{2r^2}\phi_\theta^2)\}\{\frac{1}{r}(r\phi_r)_r + \frac{1}{r^2}\phi_{\theta\theta}\}$$

$$+ \{\frac{\partial}{\partial t} + \frac{1}{2}\phi_r\frac{\partial}{\partial r} + \frac{1}{2r^2}\phi_\theta\frac{\partial}{\partial\theta}\}\{\phi_r^2 + \frac{1}{r^2}\phi_\theta^2\} = 0 \tag{2}$$

In this report, we shall consider only axisymmetric cases ($\frac{\partial}{\partial\theta} = 0$). Also, for simplicity, $\gamma - 1 \approx 0$ is assumed. Thus, equation (2) becomes

$$\phi_{tt} - (\bar{a}^2 - \phi_r^2)\phi_{rr} + 2\phi_r\phi_{rt} - \frac{\bar{a}^2}{r}\phi_r = 0 \tag{3}$$

Denoting dimensional variables with primes, nondimensional variables are defined:

$$r = \frac{r'}{R}, \quad t = t'\bar{a}/R, \quad \phi = \frac{\phi'}{\bar{a}R}$$

where R is the radius of the cylinder. The resulting non-dimensional equation is

$$\phi_{tt} - (1 - \phi_r^2)\,\phi_{rr} + 2\phi_r\phi_{rt} - \frac{1}{r}\,\phi_r = 0 \tag{4}$$

The following boundary conditions specify no flow through the cylinder wall and no flow at the cylinder axis:

$$\phi_r(1,t) = \phi_r(0,t) = 0 \tag{5}$$

The corresponding dimensionless pressure is:

$$p = e^{-(\phi_t + \frac{\phi_r^2}{2})} - 1 \tag{6}$$

where $p = p'/(\rho_o \bar{a}^2)$. ρ_o is the density of the fluid in the chamber when there is no disturbance, and $\bar{p}$ is zero if there is no disturbance in the chamber.

NUMERICAL METHOD

Characteristics

Equation (4) proves to be a hyperbolic equation. Therefore, a method of characteristics can be used for numerical solution (Ref. 5).

Let $$u \equiv \phi_t \ , \quad v \equiv \phi_r \ . \tag{7}$$

Substituting equations (7) into equation (4) yields:

$$u_t - (1 - v^2)u_r + 2v\,u_r = \frac{1}{r}\,v. \tag{8}$$

Directly from equation (7),

$$u_r = v_t \ . \tag{9}$$

If we now introduce new characteristic coordinates ξ, η, then the first derivatives with respect to r and t become:

$$\frac{\partial}{\partial r} = \xi_r \frac{\partial}{\partial \xi} + \eta_r \frac{\partial}{\partial \eta} \tag{10a}$$

$$\frac{\partial}{\partial t} = \xi_t \frac{\partial}{\partial \xi} + \eta_t \frac{\partial}{\partial \eta} \tag{10b}$$

and equations (8) and (9) become

$$\xi_t u_\xi + \eta_t u_\eta - (1 - v^2)(\xi_r v_\xi + \eta_r v_\eta) + 2v(\xi_r u_\xi + \eta_r u_\eta) = \frac{1}{r} v$$

$$\xi_r u_\xi + \eta_r u_\eta - (\xi_t v_\xi + \eta_t v_\eta) = 0$$

Thus

$$\begin{bmatrix} \eta_t + 2v\eta_r & , & -(1 - v^2)\eta_r \\ \eta_r & , & -\eta_t \end{bmatrix} \begin{bmatrix} u_\eta \\ v_\eta \end{bmatrix} = -\begin{bmatrix} u_\xi(\xi_t + 2v\xi_r) - (1 - v^2)\xi_r v_\xi - \frac{1}{r} v \\ \xi_r u_\xi - \xi_t v_\xi \end{bmatrix}$$

In order to make u_η and v_η indefinite, we have to have

$$\eta_r^2(1-v^2) - \eta_t(\eta_t + 2v\eta_r) = 0 \tag{11}$$

and

$$\eta_t[(\xi_t + 2v\xi_r)u_\xi - (1-v^2)\xi_r v_\xi - \frac{1}{r} v] - (1-v^2)\eta_r(\xi_r u_\xi - \xi_t v_\xi) = 0 \tag{12}$$

But

$$\frac{\eta_t}{\eta_r} = -\left(\frac{\partial r}{\partial t}\right)_\eta$$

and thus equation (11) becomes:

$$\left(\frac{\partial r}{\partial t}\right)_\eta^2 - 2v\left(\frac{\partial r}{\partial t}\right)_\eta - (1-v^2) = 0$$

which yields the result

$$\left(\frac{\partial r}{\partial t}\right)_{\eta} = -(1-v) \text{ or } (1+v) \qquad (13),(14)$$

The corresponding form of equation (12) is

$$\left(\frac{\partial r}{\partial t}\right)_{\eta}\left[(\xi_t + 2v\xi_r)u_\xi - (1-v^2)\xi_r v_\xi - \frac{1}{r}v\right] + (1-v^2)(\xi_r u_\xi - \xi_t v_\xi) = 0 \quad (15)$$

If $\left(\frac{\partial r}{\partial t}\right)_{\eta} = -(1-v) \neq 0$, eq. (15) becomes

$$(\xi_t + 2v\xi_r)u_\xi - (1-v^2)\xi_r v_\xi - \frac{1}{r}v - (1+v)(\xi_r u_\xi - \xi_t v_\xi) = 0$$

Thus, $[\xi_t - (1-v)\xi_r][u_\xi + (1+v)v_\xi] = \frac{1}{r}v$

And since

$$\left(\frac{\partial \xi}{\partial t}\right)_{\eta} = \left(\frac{\partial \xi}{\partial t}\right)_{r} + \left(\frac{\partial r}{\partial t}\right)_{\eta}\left(\frac{\partial \xi}{\partial r}\right)_{t} = \left(\frac{\partial \xi}{\partial t}\right)_{r} - (1-v)\xi_r$$

we have the characteristic equation

$$\left(\frac{\partial \xi}{\partial t}\right)_{\eta}\left[\left(\frac{\partial u}{\partial \xi}\right)_{\eta} + (1+v)\left(\frac{\partial v}{\partial \xi}\right)_{\eta}\right] = \frac{1}{r}v$$

or

$$\left(\frac{\partial u}{\partial t}\right)_{\eta} + (1+v)\left(\frac{\partial v}{\partial t}\right)_{\eta} = \frac{1}{r}v$$

If, on the other hand, $\left(\frac{\partial r}{\partial t}\right) = 1 + v \neq 0$, then

$$\xi_t[u_\xi - (1-v)v_\xi] + \xi_r[2vu_\xi - (1-v)v_\xi + (1-v)u_\xi] = \frac{1}{r}v$$

and in a similar manner, we obtain the second of the pair of characteristic equations:

$$\frac{\partial u}{\partial t} + (1 + v)\frac{\partial v}{\partial t} = \frac{1}{r} v \quad \text{on} \quad \frac{\partial r}{\partial t} = -(1 - v) \neq 0 \tag{16a}$$

$$\frac{\partial u}{\partial t} - (1 - v)\frac{\partial v}{\partial t} = \frac{1}{r} v \quad \text{on} \quad \frac{\partial r}{\partial t} = (1 + v) \tag{16b}$$

The pressure field is, (from Eq. (6))

$$p = \exp[-(u + \frac{v^2}{2})] - 1. \tag{17}$$

Numerical Calculation (Ref. 6)

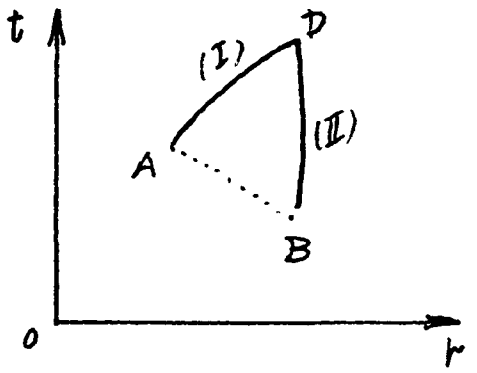

Fig. 1. Finding a new mesh point. Characteristics - AD and - BD are of opposite families.

In all cases, the differential coefficients are replaced by the divided differences over an interval, and other quantities are replaced by the arithmetic mean over the interval. For example, over the range AD in Fig. 1, the equation $\frac{dr}{dt} = 1 + v$ will be replaced by the equation $r_D - r_A = [1 + v]_{AD}(t_D - t_A)$ where $[1 + v]_{AD}$ signifies an arithmetic mean over the interval A and D i.e., $1 + 1/2\ (v_A + v_D)$.

Suppose we know all values v, u, t and r at points A and B; then we can find these values at point D as follows: Eq. (16) is replaced by

$$r_D - r_A = [1 + v]_{AD}\ (t_D - t_A) \tag{18}$$

$$r_D - r_B = -[1 - v]_{BD}\ (t_D - t_B) \tag{19}$$

$$u_D - u_A + [v - 1]_{AD}\ (v_D - r_A) = (t_D - t_A) \int_A^D \frac{1}{r} v dt^* \tag{20}$$

$$u_D - u_B + [v + 1]_{BD}\ (v_D - v_B) = (t_D - t_B) \int_B^D \frac{1}{r} v dt^* \tag{21}$$

And from eqs. (18) and (19),

---

* For the calculation of this integral, see Appendix A.

$$t_D = \frac{r_B - r_A + t_A[v+1]_{AD} - t_B[v-1]_{BD}}{[v+1]_{AD} - [v-1]_{BD}} \tag{22}$$

$$r_D = r_A + [v+1]_{AD}(t_D - t_A) \tag{23}$$

Also, from eqs. (20) and (21),

$$v_D = \frac{\int_A^D \frac{1}{r}\,vdt \times (t_D - t_A) - (t_D - t_B)\int_B^D \frac{1}{r}\,vdt + v_A[v-1]_{AD} - v_B[v+1]_{BD} + u_A - u_B}{[v-1]_{AD} - [v+1]_{BD}} \tag{24}$$

$$u_D = u_A - [v-1]_{AD}(v_D - v_A) + \int_A^D \frac{1}{r}\,vdt \times (t_D - t_A) \tag{25}$$

Thus, we can find the values of u, v, r and t at the new point. Furthermore, using the foregoing equations, if we know all the information at the points 1, 2, ... , 10 on line A-A' of Fig. 2, we can calculate new values at the points 1', 2, ... , 10" on line BB'.

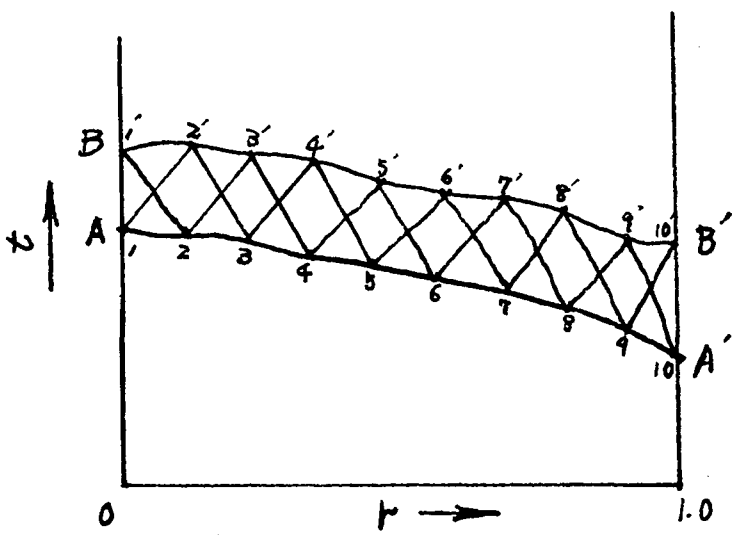

Fig. 2. Grid of characteristics illustrating the process of calculation from the known state AA' to the new state BB'.

Shock Occurrence

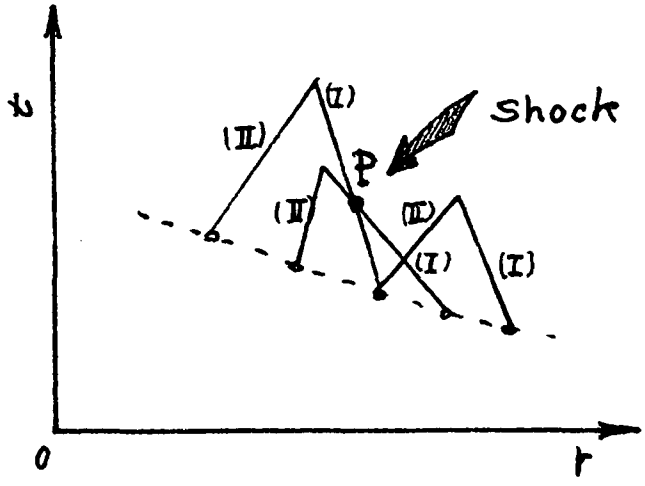

Fig. 3. A shock occurrence, where two characteristics of the same family cross. (At point P, 2 characteristics of family (I) are crossing.)

A shock is taken to be indicated by the intersection of two characteristic lines of the same family. Following such an occurrence, the development of a shock will obey the Rankine-Hugoniot conditions. In this paper, the object is to find the possibility of the shock formation as a function of wave amplitude. Therefore, the calculations do not consider the propagation of the shock after it has first been indicated by coalescence of characteristics. However, it may be noted that, in our method, the time level at each stage of calculations is not the same. Therefore, in order to describe the wave shape at the time the shock is first indicated, additional calculations are needed to fill the empty (t,r) space up to that time. Referring to Fig. 4, the upper right hand side (cross hatched part) must be filled in.

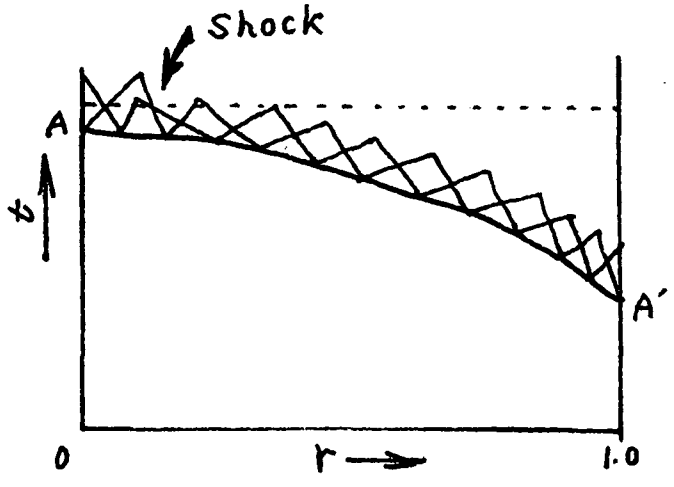

Fig. 4. Distribution of grid points when shock is indicated.

Initial Conditions

Equation (4) is non-linear; therefore, the choice of initial condition is very important for this particular study. For example, if a function with singularities in the first derivatives is picked as an initial velocity distribution, then a shock may occur very early at a very small magnitude. In order to provide a suitable variety of initial conditions, the following three problems are posed:

(a) Use the power-series solution (see ref. [4] and also Appendix A) to the 2nd order approximation as an initial condition

$$\phi = \varepsilon\phi^{(1)} + \varepsilon^2\phi^{(2)} + \ldots \tag{26}$$

and perform calculations for various values of initial amplitude ε.

(b) Use the solution of the power series to the 2nd order approximation with the velocity magnitude = 0.1 as initial condition and put the velocity disturbance at the outer boundary as a function of pressure at the wall, $v_{wall} = -\sigma p$ (ref. [3]):

$$v_{wall} = -\sigma \cdot p \tag{27}$$

This gives a gradual amplification of the transverse oscillation and the rate of this magnification depends on the coefficient σ. This case corresponds to the response of a vigorous burning zone near the wall. This response may be considered to provide a simple model of combustion instability.

(c) Start with the procedure of case (b), but after the magnitude of the oscillation reaches some prescribed value, then stop the amplification (set $\sigma = 0$) and watch the oscillation proceed. By this technique, the direct effect of the wall amplification condition on the shock formation may be minimized. Also, such an amplification cut-off would represent the limiting effects of unspecified damping mechanisms. Further, using small values of σ should also minimize any direct effects of amplification rates on the waves.

Error Estimation

There are no constraints imposed on the spatial mesh size, and Δt is automatically determined once the spatial grid size is given.

By using a Taylor series analysis of the equations, truncation errors for each equation can be estimated.

$$\left(\frac{\partial r}{\partial t}\right)_{\eta} = v - 1 \tag{13}$$

The Taylor series is

$$r_{i+1} = r_i + \frac{\partial r}{\partial t})_{\eta,i} \Delta t + \frac{1}{2} \frac{\partial^2 r}{\partial t^2})_{\eta,i} \Delta t^2 + 0(\Delta t^3)$$

$$r_i = r_{i+1} - \frac{\partial r}{\partial t})_{\eta,i+1} \Delta t + \frac{1}{2} \frac{\partial^2 r}{\partial t^2})_{\eta,i+1} \Delta t^2 + 0(\Delta t^3) \qquad (28)$$

$$r_{i+1} - r_i = \frac{1}{2}[\frac{\partial r}{\partial t})_{\eta,i} + \frac{\partial r}{\partial t})_{\eta,i+1}] \Delta t + \frac{1}{4}[\frac{\partial^2 r}{\partial t^2})_{\eta,i} - \frac{\partial^2 r}{\partial t^2})_{\eta,i+1}]\Delta t^2 + 0(\Delta t^3)$$

Applying Eq. (13) for both points i and i+1, we get

$$\frac{\partial r}{\partial t})_{\eta,i+1} = v_{i+1} - 1$$

$$\frac{\partial r}{\partial t})_{\eta,i} = v_i - 1$$

We add above two equations and divide by 2:

$$\frac{1}{2}[\frac{\partial r}{\partial t})_{\eta,i+1} + \frac{\partial r}{\partial t})_{\eta,i}] = [v - 1]_{i,i+1} \qquad (29)$$

Comparing Eq. (28) and (29) gives the truncation error:

$$TE = \frac{1}{4} [\frac{\partial^2 r}{\partial t^2})_{\eta,i} - \frac{\partial^2 r}{\partial t^2})_{\eta i+1}]\Delta t + 0(\Delta t^2) \qquad (16a)$$

Integrating eq. (16a) gives

$$u_{i+1} - u_i + [\frac{1}{2} v + v]_{i+1} - [\frac{1}{2} v + v]_i = \int_i^{i+1} \frac{1}{r} v \, dt$$

$$u_{i+1} - u_i + (u_{i+1} - v_i)[\frac{1}{2} (v_{i+1} + v_i) + 1] = \int_i^{i+1} \frac{1}{r} v \, dt$$

whence:

$$u_{i+1} - u_i + (v_{i+1} - v_i)[1 + v]_{i,i+1} = \int_i^{i+1} \frac{1}{r} v \, dt$$

Truncation error for this equation is only that for the integration. (See Appendix B)

For the integration, the assumption is made that the velocity profile between 2 grids (i & i + 1) is linear, i.e.,

$$v_o = v_i + \frac{v_{i+1} - v_i}{\Delta r} \Delta r_1$$

But a Taylor Series expansion yields

$$v_o = v_i + \frac{v_{i+1}-v_i}{\Delta r} \Delta r_1 - \frac{1}{2} \frac{\partial^2 v}{\partial r^2}_o \Delta r_1 (\Delta r - \Delta r_1) + 0(\Delta r^3).$$

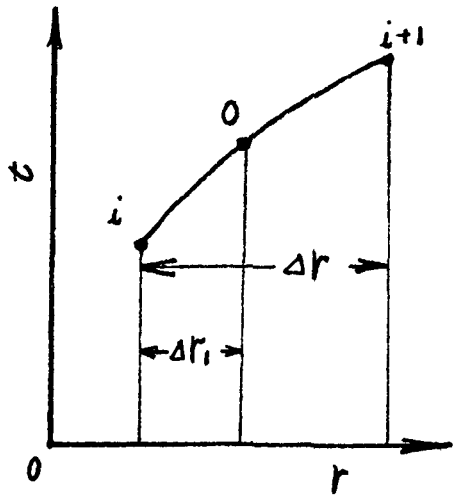

Fig. 5. A characteristic line between 2 grid points i and i+1. 0 is a point on this characteristic line.

So the error in the velocity due to the linear assumption is

$$E = 0[\frac{1}{2}(\frac{\partial^2 v}{\partial r^2})_o \cdot \Delta r_1 (\Delta r - \Delta r_1)]$$

$$< 0[\frac{1}{8}(\frac{\partial^2 v}{\partial r^2})_{max} \cdot \Delta r^2]$$

where $(\frac{\partial^2 v}{\partial r^2})_{max}$ is the maximum value of $\frac{\partial^2 v}{\partial r^2}$ on the characteristic line between i and i + 1. As is shown in Appendix A, the integration was carried out as follows.

$$\int_i^{i+1} \frac{1}{r} v \, dt = \int_i^{i+1} \frac{v}{r} \frac{dr}{[v+1]_{i,i+1}} = \frac{1}{[v+1]_{i,i+1}} \int_i^{i+1} \frac{v}{r} dr$$

Thus, the resulting truncation error is of order:

$$T.E. \sim 0[\frac{1}{8} (\frac{\partial^2 v}{\partial r^2})_{max} \frac{1}{[v+1]_{i,i+1}} \frac{\Delta r^3}{r}]$$

RESULTS

For all calculations, 51 grid points are chosen. Thus, Δr is 0.02 initially.

Case (a). - The following calculations were performed for initial conditions given by two terms of a power series in ε (eq. (26)):

Table 1: Shock occurrences for various initial wave magnitudes.

Initial Magnitude*	ε	Shock	At Time $(R/\bar{a}_o)$
0.1	(4.485×10^{-2})	No	--
0.175	(7.849×10^{-2})	No	--
0.195	(8.746×10^{-2})	Yes	13.5
0.200	(8.970×10^{-2})	Yes	5.2
0.250	(1.1213×10^{-1})	Yes	2.2
0.300	(1.3456×10^{-1})	Yes	1.5
0.350	(1.5698×10^{-1})	Yes	1.3

Fig. 6 shows the behavior of a wave with initial magnitude 0.30 ($\varepsilon = 0.1346$). From this figure and with the table above, it is clear that as time goes on, a sharp wave front appears for the waves which have comparatively large initial magnitudes and the crests grow, eventually being followed by shock formation.

Changes of wave magnitude with time for each initial magnitude is described in Fig. 7. By magnitude is meant the highest wave amplitude during a half-cycle of wave oscillation. Every wave increases its magnitude at first, but lower magnitude waves often reach a certain amplitude, decay almost to their own initial conditions. Waves repeat this process with a period almost equal to three times that of the wave oscillation period.

The amplitude of this magnitude change is of order $(\varepsilon\beta)^3$, i.e., 3rd order in the power series for velocity. Since there is no damping factor like viscosity in this problem, the difference between initial condition and the

---

* Definition of Magnitude (see also Appendix B): Magnitude = 0.581864 $(\varepsilon\beta)$, where β is the first zero of first order Bessel function, i.e., $J_1(\beta) = 0$.

exact solution for the differential equation does not attenuate and presumably causes these fluctuations of wave magnitude. Fig. 8 indicates the possibility

Table 2: Order of the change of wave magnitude. $(\varepsilon\beta)^3$ is the order of the 3rd order approximation of the power series solution for velocity.

Initial Magnitude	$(\varepsilon\beta)^3$	Δ (Magnitude of Wave)
0.1	0.0051	~ 0.0025
0.175	0.0272	~ 0.025
0.195	0.0378	~ 0.045
0.200	0.0407	~ 0.050

of the existance of a wave magnitude above which the wave grows to a shock, but below which it oscillates in the cylinder forever. An initial wave magnitude around 0.180 seems to be the borderline for this particular initial condition. (ε value of the series is 0.08.)

Due to the irregularity of this oscillation, we failed in the attempt to find a repetition of identical wave patterns after a certain number of cycles for an initial magnitude of 0.175. However, as seen in Fig. 9, the wave shape of magnitude 0.175 after 16 cycles still is not steep at all. At least this helps to justify our conclusion that no shock occurs.

Convergence and stability of the finite difference scheme were also checked to determine if round-off or truncation error could be the source of fluctuations of wave magnitude. In Fig. 10, comparison is made between calculations with 51 grid points and with 76 grid points for the initial velocity magnitude 0.175. The results show that the effect of the increment in number of grid points is almost negligible, and imply the convergence of the finite difference scheme. As for round-off error, calculations with double-precision accuracy were made at the wave magnitude 0.7 and the results are shown in the following table. After 243 calculation steps, the difference is still $0(10^{-5})$ and very small. Thus the finite difference scheme is very stable.

Table 3: Effect of round-off error; single precision (accuracy of 7 decimals) and double precision (accuracy of 16 decimals).

Time Steps	Position (Double)	Time	Velocity	Pressure
0			Initial Condition	
53	0.488473 (0.488490)	1.05907 (1.05909)	0.544833×10^{-1} $(0.544851 \times 10^{-1})$	-0.445474×10^{-1} $(-0.445476 \times 10^{-1})$
103	0.474543 (0.474523)	2.06016 (2.06021)	0.510547×10^{-2} $(0.511077 \times 10^{-2})$	0.426178×10^{-1} $(0.426278 \times 10^{-1})$
143	0.482243 (0.482259)	3.06948 (3.06952)	-0.643517×10^{-1} $(-0.643588 \times 10^{-1})$	-0.397105×10^{-1} $(-0.397099 \times 10^{-1})$
193	0.474554 (0.474553)	4.03490 (4.03493)	0.997936×10^{-1} $(0.998079 \times 10^{-1})$	0.213518×10^{-1} $(0.213533 \times 10^{-1})$
243	0.473359 (0.473345)	5.03056 (5.03058)	-0.923763×10^{-1} $(-0.923878 \times 10^{-1})$	0.313444×10^{-1} $(0.313555 \times 10^{-1})$

Case (b). - For oscillations driven by wall amplification (eq. (27)), six of σ values were chosen and the results are shown in Fig. 11-A and B.

Table 4: Shock occurrences for various rates of wall amplification.

σ	Shock		
	Time	Position	Magnitude
0.20	5.1	0.14	0.356
0.15	6.1	0.92	0.307
0.10	11.1	0.74	0.390
0.05	18.3	0.003	0.361
0.03	31.1	0.07	0.355
0.01	72.2	0.08	0.238

A shock is most likely to occur at the center, but now the boundary condition $v = -\sigma p$ is introduced at the outer surface. Thus, when the wave is moving inward towards the center of the cylinder, it is at the same time being pulled back at the wall, decreasing the energy flow toward the center. Thus, until the strength of the wave gets big enough to overcome this pullback, a shock will not be generated. That is the reason why the shock is developed at such a high magnitude in this case in contrast to cases (a) and (c) below.

When σ is below 0.05, a weak shock is generated almost at the center of the cylinder and is different from the ones when σ is above 0.1. Figs. 12 and 13 show the wave patterns for $\sigma = 0.05$ and $\sigma = 0.1$ just before the shock is generated. Also Fig. 14 shows the process of wave amplification for these two cases.

In the case $\sigma = 0.01$, the amplification of wave magnitude is very small, as can be seen in Figs. 11-A and B. But still a shock is generated. This implies that the power series converges up to a certain value of ε, and this ε is no bigger than 0.090 (magnitude of velocity $\doteqdot 0.2$).

Case (c). - In this case, the value $\sigma = 0.05$ is chosen and the amplification is stopped at various times but always when most of the kinetic energy is transferred into potential energy. Thus, all actions of stopping amplification occur at the same phase of the oscillation.

Figs. 15 and 16 show the results. In Fig. 16 time is measured from the time when the amplification is stopped. Thus, $t = 0$ line in Fig. 16 is equivalent to the $\sigma = 0.05$ line in Fig. 15.

Compared to Case (a), this case has much less fluctuation of magnitude, as was anticipated. From Fig. 16, one can see that the largest magnitude at which a transverse wave canoscillate in the cylinder without growing into a shock is somewhwere around 0.13 ($\varepsilon \doteqdot 0.058$). This figure is a little smaller than the result obtained for Case (a) (0.18). Thus the history of the oscillation must be an important factor in this problem.

For all cases (a,b, and c), it appears that there exists a permanent potential form for this resonant mode of transverse oscillation in the circular cylinder for sufficiently small but finite values of ε.

For the purpose of checking whether the above results are sensitive to the value of σ, one calculation was made stopping amplification around velocity magnitude 0.2 for the case of $\sigma = 0.01$. The result is shown in Fig. 11-B. A shock is still generated in this case at the position $R = 0.14$. So we may conclude that the above results are quite independent of the value of σ, as long as σ is reasonably small.

CONCLUSION

Numerical solutions have been obtained for the one-dimensional resonant mode ($n = 0$) of the nonlinear oscillation transverse to the axis of a circular cylinder.

Three types of calculations are performed, and each indicates the existence of a permanent potential form for this resonant mode ($n = 0$). There is apparently a critical value of ε for the power series to converge. The value is around $0.06 \approx 0.08$. Above this value, the wave develops a shock pattern, but below it, the wave oscillates in the cylinder for an indefinite time, probably permanently, as suggested in Refs. 3 and 4.

BIBLIOGRAPHY

1. Crocco, Luigi, and Cheng, Sin I., High Frequency Combustion Instability in Ricket Motor with Concentrated Combustion, J. Am. Rocket Soc., Vol. 23, No. 5, pp. 301-313, Sept.-Oct., 1953.

2. Grad, Harold, Resonance Burning in Rocket Motors, Communications on Pure and Applied Mathematics, Vol. 2, No. 1, pp. 79-102, March, 1949.

3. Moore, Franklin K. and Maslen, Stephen H., Transverse Oscillations in a Cylindrical Combustion Chamber, NACA TN 3152, 1954.

4. Maslen, Stephen H. and Moore, Franklin K., On Strong Transverse Waves without Shocks in a Circular Cylinder, J. Aeronautical Sciences, pp. 583-592, June, 1956.

5. Mathews, J. and Walker, R.L., Mathematical Methods of Physics, W.A. Benjamin, Inc., pp. 210-217, 1965.

6. Hoskin, N.E., Solution by Characteristics of the Equation of One-dimensional Unsteady Flow, Methods in Computational Physics (III), Academic Press, pp. 265-293, 1964.

APPENDIX A

Calculation of Integral $\int_A^D \frac{1}{r} v\,dt$ and $\int_B^D \frac{1}{r} v\,dt$

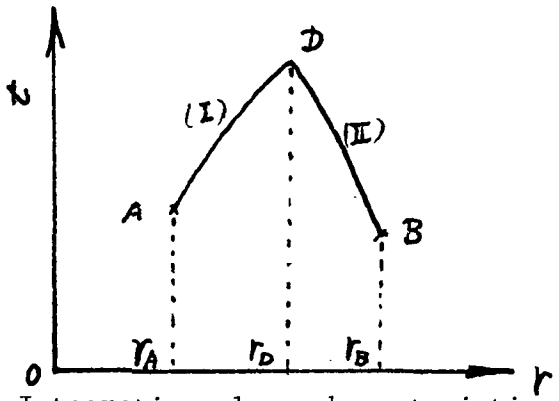

Integration along characteristic lines AD and BD.

On the line AD, we have

$$dr = [1 + v]_{AD}\, dt.$$

Thus, the integration becomes,

$$\int_A^D \frac{1}{r} v\,dt = \frac{1}{[1+v]_{AD}} \int_A^D \frac{v}{r}\, dr \qquad (A\text{-}1)$$

Assuming linear velocity profile along the characteristic line AD, we can evaluate the integral. The result is,

$$\int_A^D \frac{1}{r} v\,dt = \frac{1}{[1+v]_{AD}} \left\{(V_D - V_A) + \left[V_A - \frac{r_A(V_D - V_A)}{r_D - r_A}\right] \cdot \ln\left(\frac{r_D}{r_A}\right)\right\}$$

* In the case when point A is at the center of the cylinder, i.e. $r_A = 0$, we have

$$\int_A^D \frac{1}{r} v\,dt = \frac{V_D}{[1+v]_{AD}} .$$

In a similar way, we can integrate the equation on the line BD.

$$\int_B^D \frac{1}{r} v\,dt = \frac{1}{[v-1]_{BD}} \left\{(V_D - V_B) - \left[V_D - \frac{r_D(V_B - V_D)}{r_B - r_D}\right] \cdot \ln\left(\frac{r_B}{r_D}\right)\right\}$$

* In the case when point D is at the center of the cylinder, i.e., $r_D = 0$, we have,

$$\int_B^D \frac{1}{r} v\,dt = \frac{V_B}{[1-v]_{BD}} .$$

APPENDIX B

The equation is

$$\phi_{tt} - (1 - \phi_r^2)\,\phi_{rr} = 2\phi_r\phi_{rt} = \frac{1}{r}\,\phi_r$$

subject to $\phi_r(1,t) = \phi_r(0,t) = 0.$

We expand the velocity potential in a power series in amplitude parameter ε:

$$\phi = \varepsilon\phi^{(1)} + \varepsilon^2\phi^{(2)} + \ldots. \qquad \text{(B-1)}$$

Then, the first order equation is

$$\phi_{tt}^{(1)} - \phi_{rr}^{(1)} - \frac{1}{r}\,\phi^{(1)} = 0$$

with the following boundary conditions:

$$\phi_r^{(1)}(1,t) = \phi_r^{(1)}\,(0,t) = 0$$

From the boundary conditions,

$$\phi^{(1)} = g(t)\; j_0\;(\beta r)$$

where β is a constant such that $J_1(\beta) = 0$, i.e., $\beta = 3.83171$. Also, $g(t)$ will be cos (βt) or sin (βt), so we can get a solution in the form,

$$\phi^{(1)} = \cos\,(\beta t)\; J_0(\beta r) \qquad \text{(B-2)}$$

The second order equation is

$$\phi_{tt}^{(2)} - \phi_{rr}^{(2)} - \frac{1}{r}\,\phi_r^{(2)} = -\,2\phi_r^{(1)}\phi_{rt}^{(1)}$$

Introducing eq. (B-2) into the above equation yields

$$\phi_{tt}^{(2)} - \phi_{rr}^{(2)} - \frac{1}{r}\phi_{r}^{(2)} = \beta^3 J_1^2 (\beta r) \sin (2\beta t)$$

By the same technique of separation of variables,

$$\phi^{(2)} = \beta f(r) \sin (2\beta t). \tag{B-3}$$

and, for the function f(r),

$$f_{rr} + \frac{1}{r} f_r + 4\beta^2 f = - \beta^2 J_1^2 (\beta r) \tag{B-4}$$

with the boundary conditions:

$$f_r(0) = f_r(1) = 0$$

Using a Green's-Function method, the inhomogeous Bessel's equation (B-4) is solved:

$$f_L = J_0 (2\beta r)$$

$$f_R = J_0 (2\beta r) - \frac{J(2\beta)}{Y(2\beta)} T_0 (2\beta r)$$

The Wronskian is

$$w = - \frac{2}{\pi r} \frac{J(2\beta)}{Y(2\beta)}$$

Then

$$f = \frac{\pi}{2} \{ \int_0^{\beta} x J_0(2x) J_1^2 (x) dx \frac{Y_1(2\beta)}{J_1(2\beta)} J_0 (2\beta r)$$

$$- \int_0^{\beta r} x J_0(2x) J_1^2 (x) dx Y_0(2\beta r)$$

$$- \int_{\beta r}^{\beta} x J_1^2 (x) Y_0 (2x) dx J_0 (2\beta r) \} \tag{B-5}$$

The integrations in eq. (B-5) are carried out by using the trapezoidal rule. Thus the solution of the original equation, to second order, is,

$$\phi = \varepsilon \cos(\beta t) J_0(\beta r) + \varepsilon^2 \beta \sin(2\beta t) f(r) \tag{B-6}$$

where f(r) is given by Eq. (B-5). Then initial conditions (at t = 0) for u and v are

$$u = \phi_t (t = 0) = 2(\beta\varepsilon)^2 f(r)$$

$$v = \phi_r (t = 0) = -(\varepsilon\beta) J_1(\beta r) \tag{B-7}$$

and the magnitude of the initial wave pattern is defined by

$$\text{Mag.} = 0.581864\ (\varepsilon\beta).$$

Also, the magnitude of wave over a certain cycle is defined by the largest amplitude of the wave during the period.

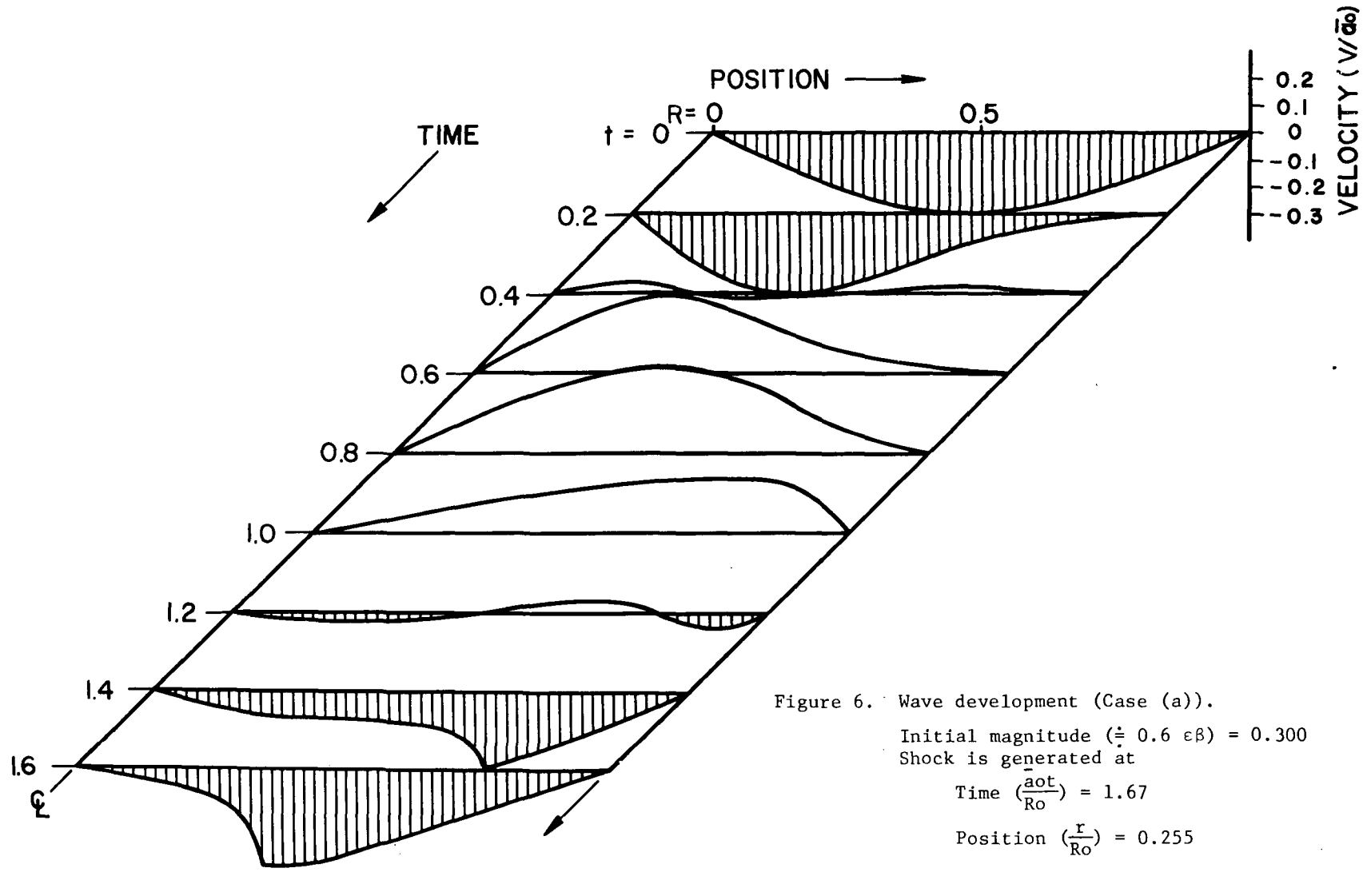

Figure 6. Wave development (Case (a)).

Initial magnitude ($\doteq 0.6\ \varepsilon\beta$) = 0.300
Shock is generated at

Time $(\frac{\bar{a}ot}{Ro})$ = 1.67

Position $(\frac{r}{Ro})$ = 0.255

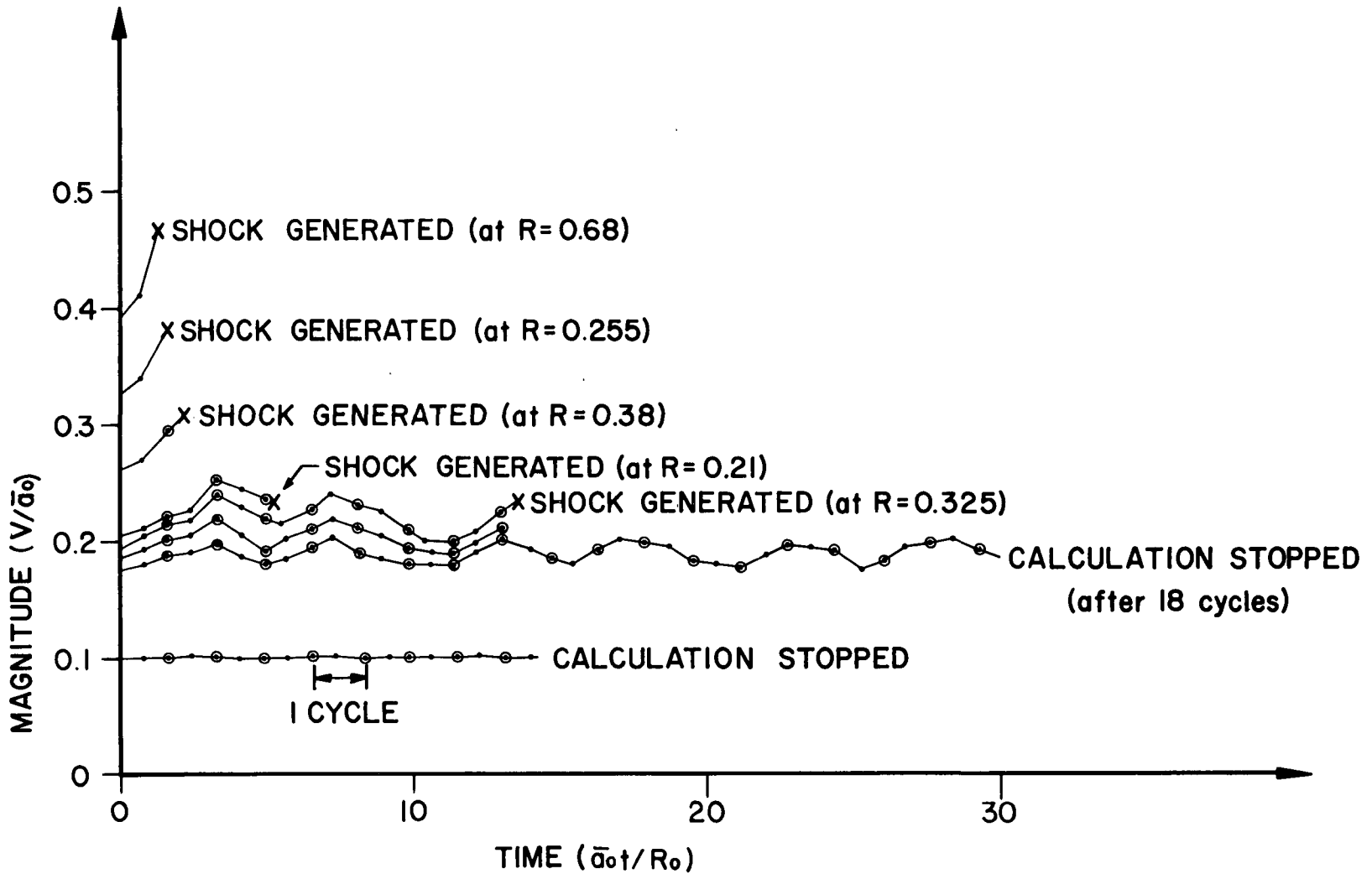

Figure 7. Shock occurrences for various initial wave magnitudes of case (a). Here, $R = r/R_o$.

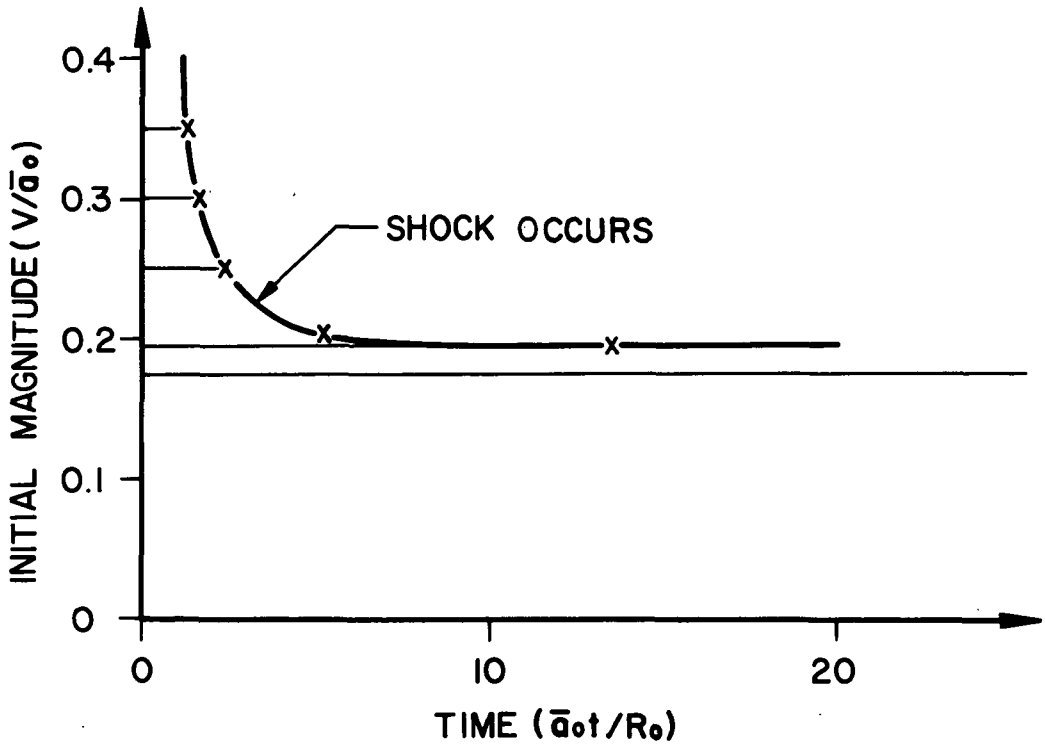

Figure 8. Estimate of the initial wave magnitude at which oscillation is permanent, for case (a).

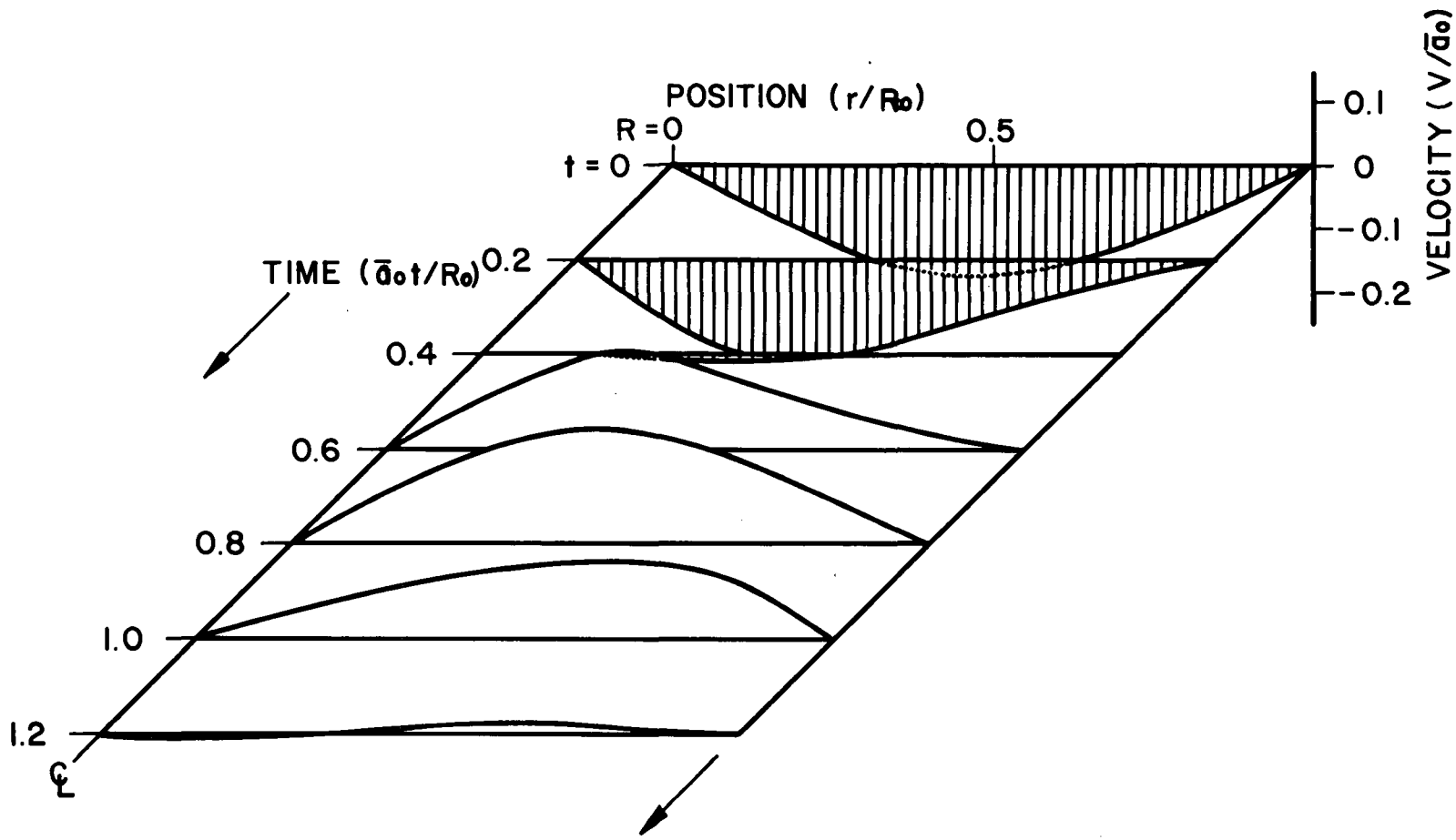

Figure 9-A. Initial wave pattern of magnitude 0.175 for case (a).

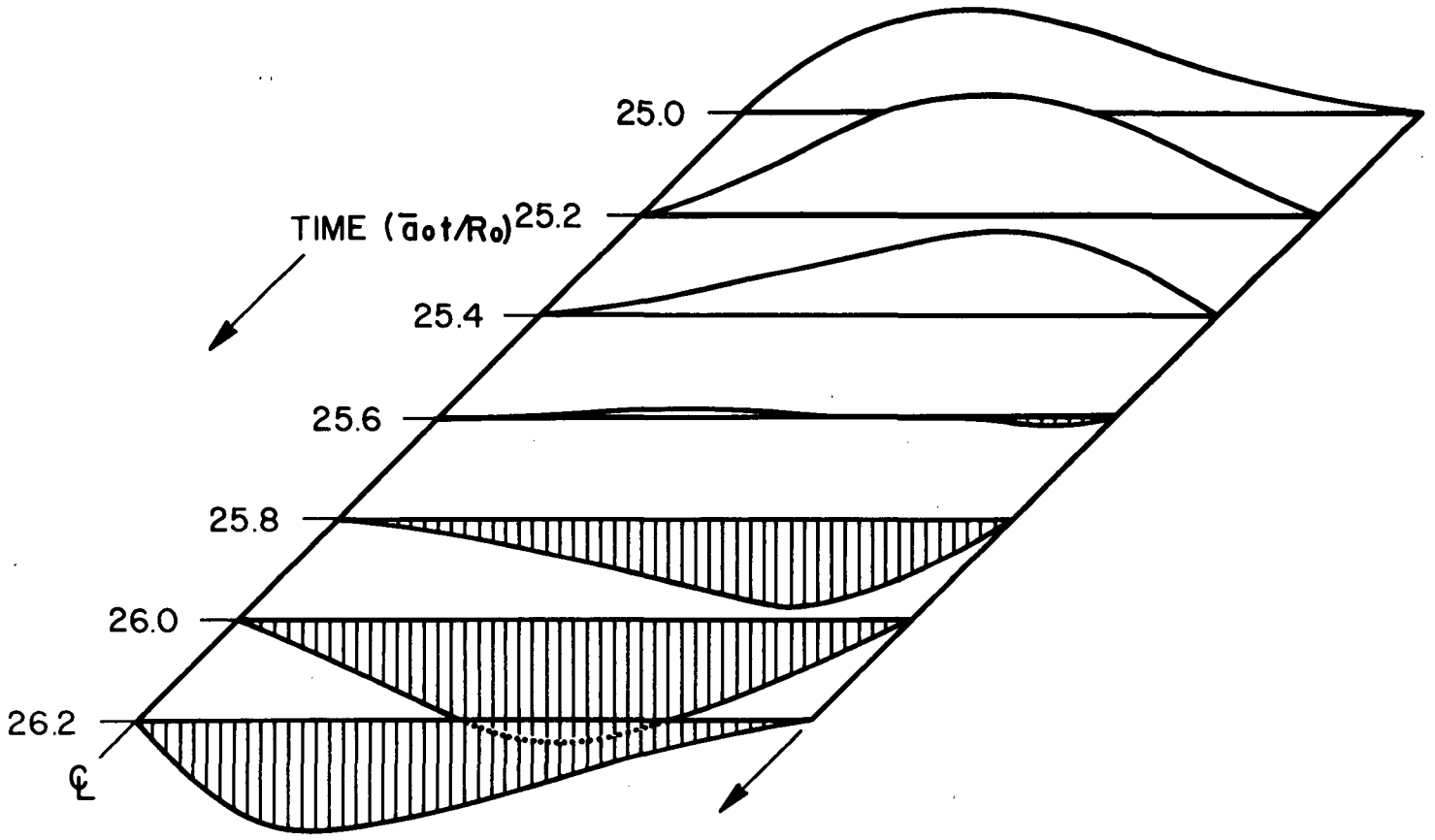

Figure 9-B. Shape of the wave in Figure 9-A,16 cycles later.

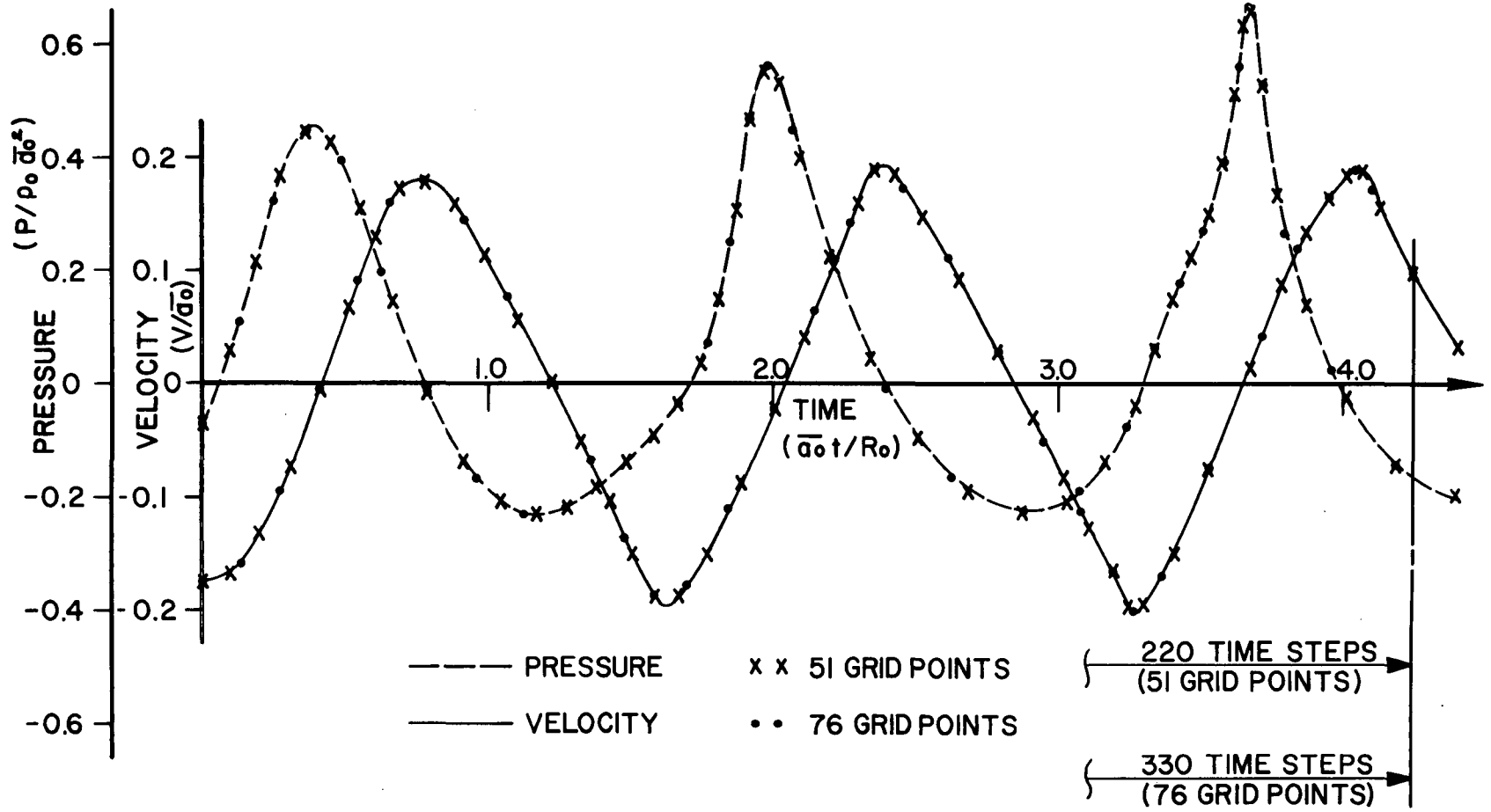

Figure 10. Convergence test for the wave of case (a) with initial velocity magnitude 0.175.

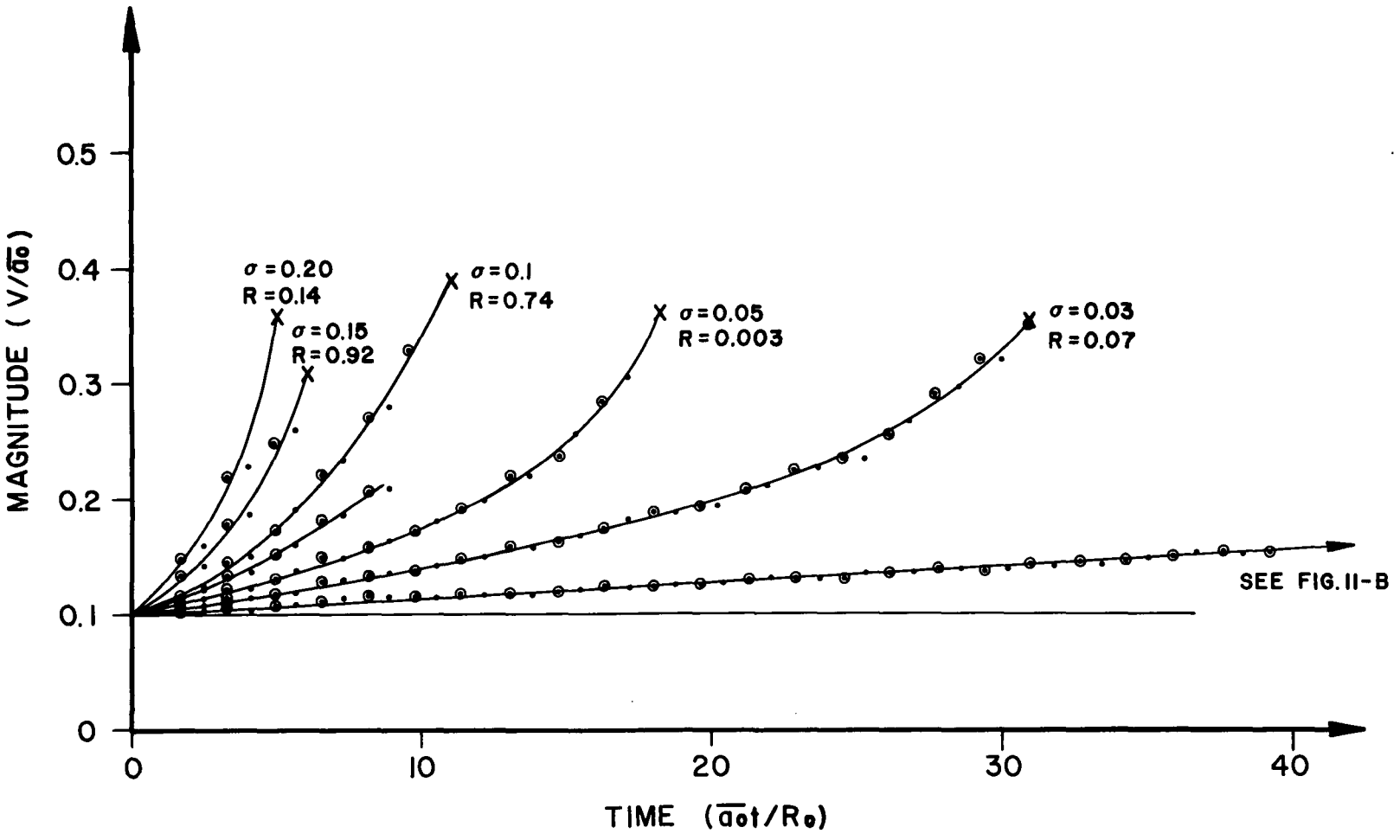

Figure 11-A. Wave amplifications and shock occurrences for case (b). Boundary condition at the wall is: $v_w = -\sigma p_w$.

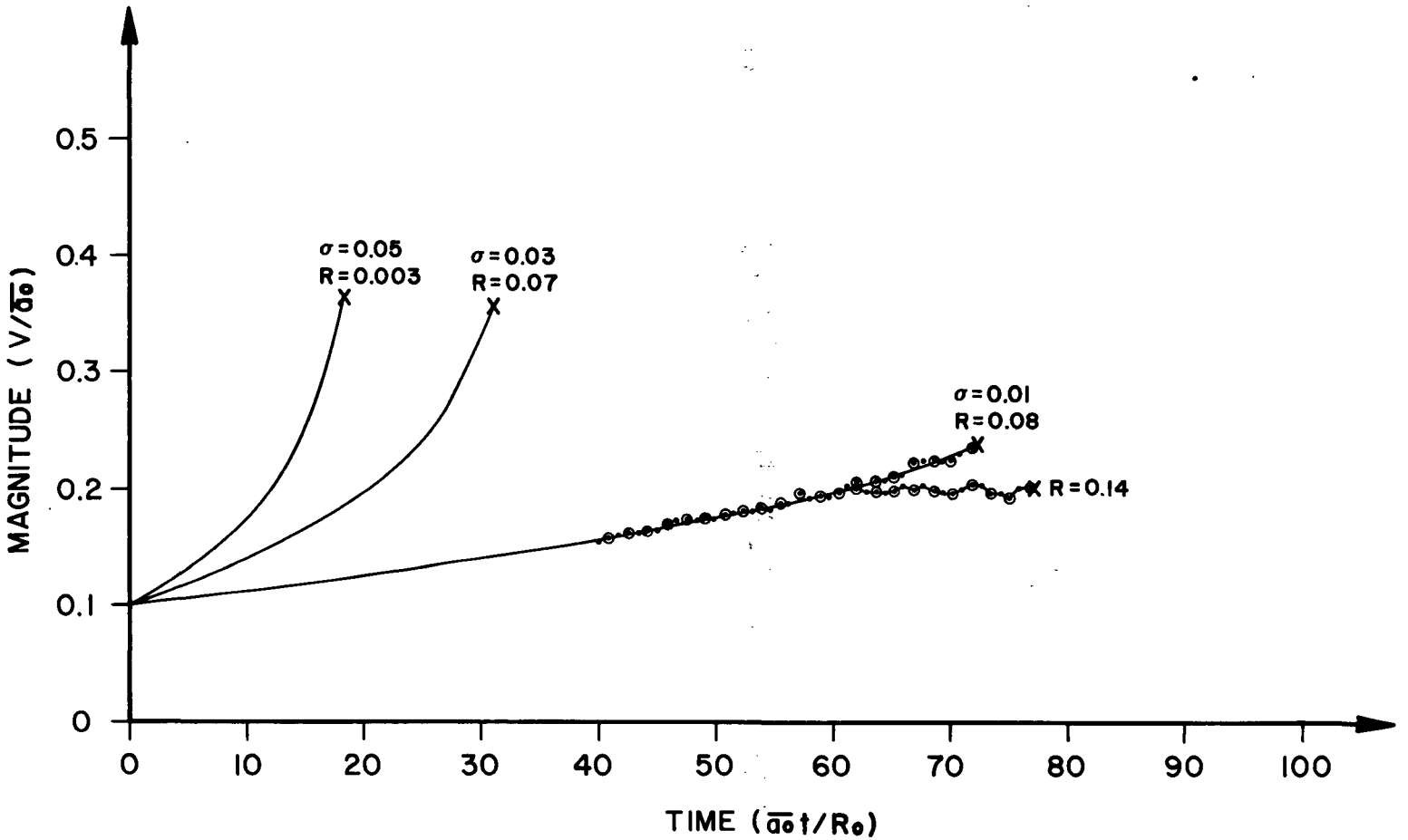

Figure 11-B. Wave amplifications and shock occurrences for case (b). Boundary condition at the wall is: $v_w = -\sigma p_w'$.

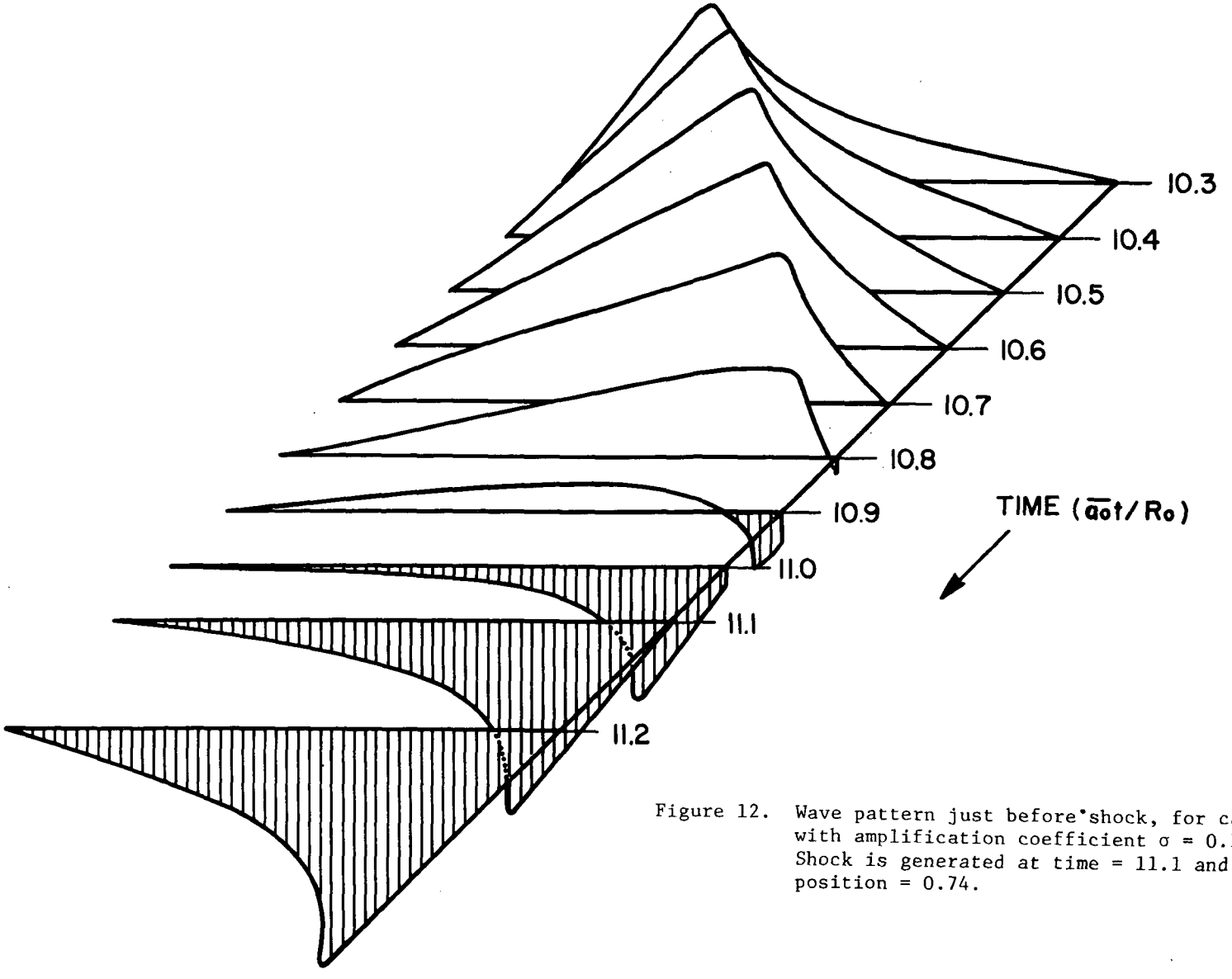

Figure 12. Wave pattern just before shock, for case (b) with amplification coefficient $\sigma = 0.1$. Shock is generated at time = 11.1 and position = 0.74.

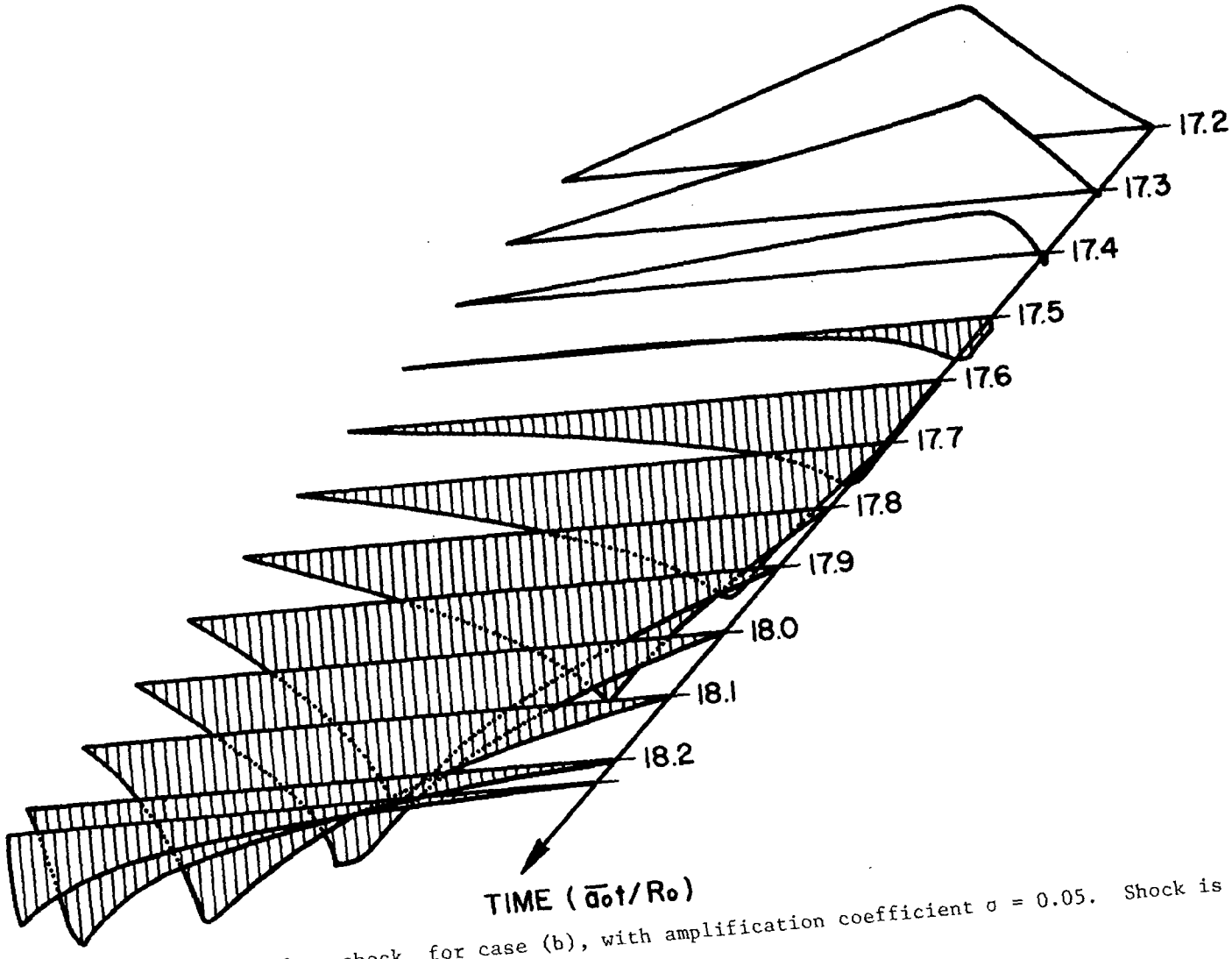

Figure 13. Wave pattern just before shock, for case (b), with amplification coefficient $\sigma = 0.05$. Shock is generated at time = 18.2 and position = 0.003.

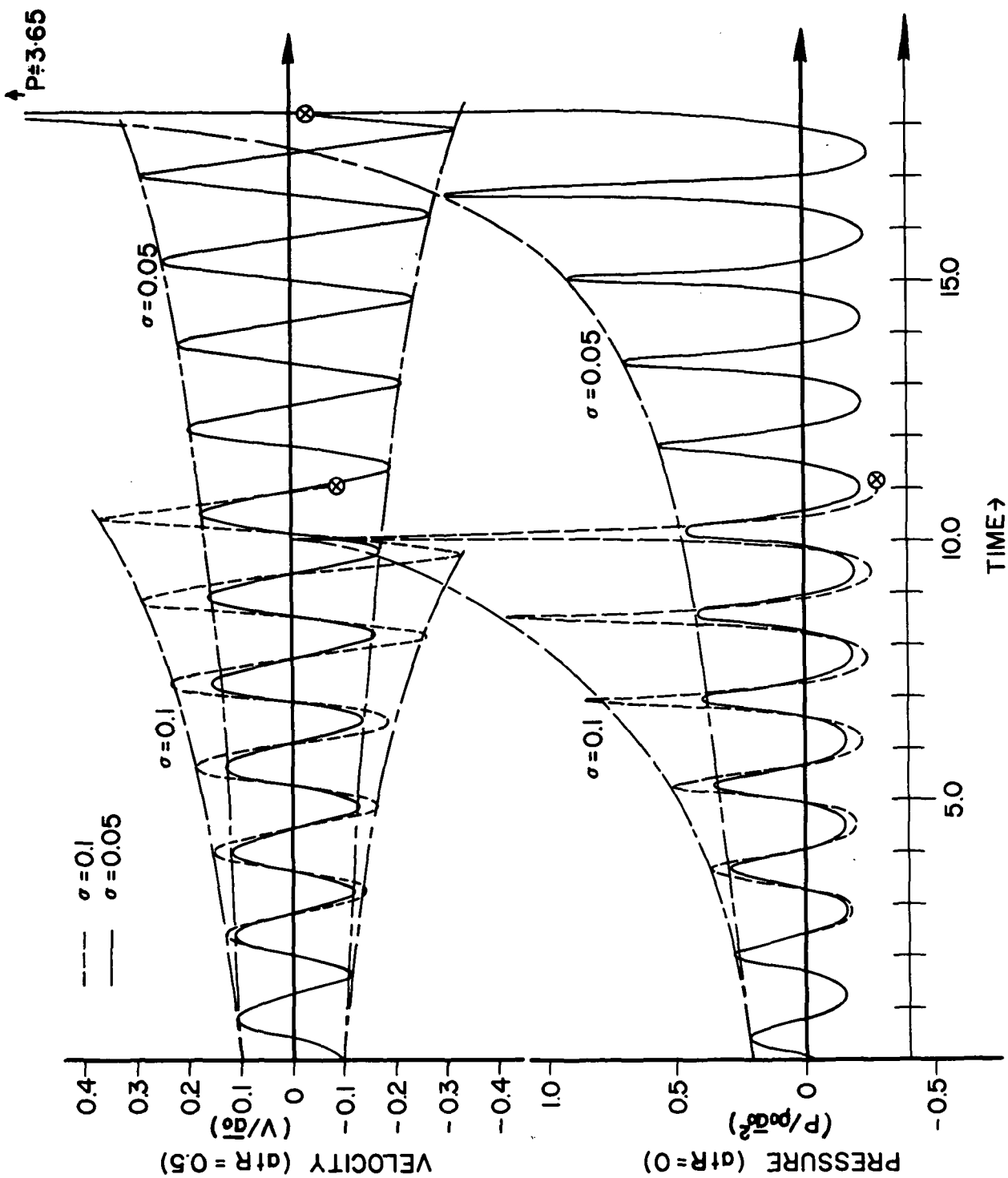

Figure 14. Wave amplification process for case (b).

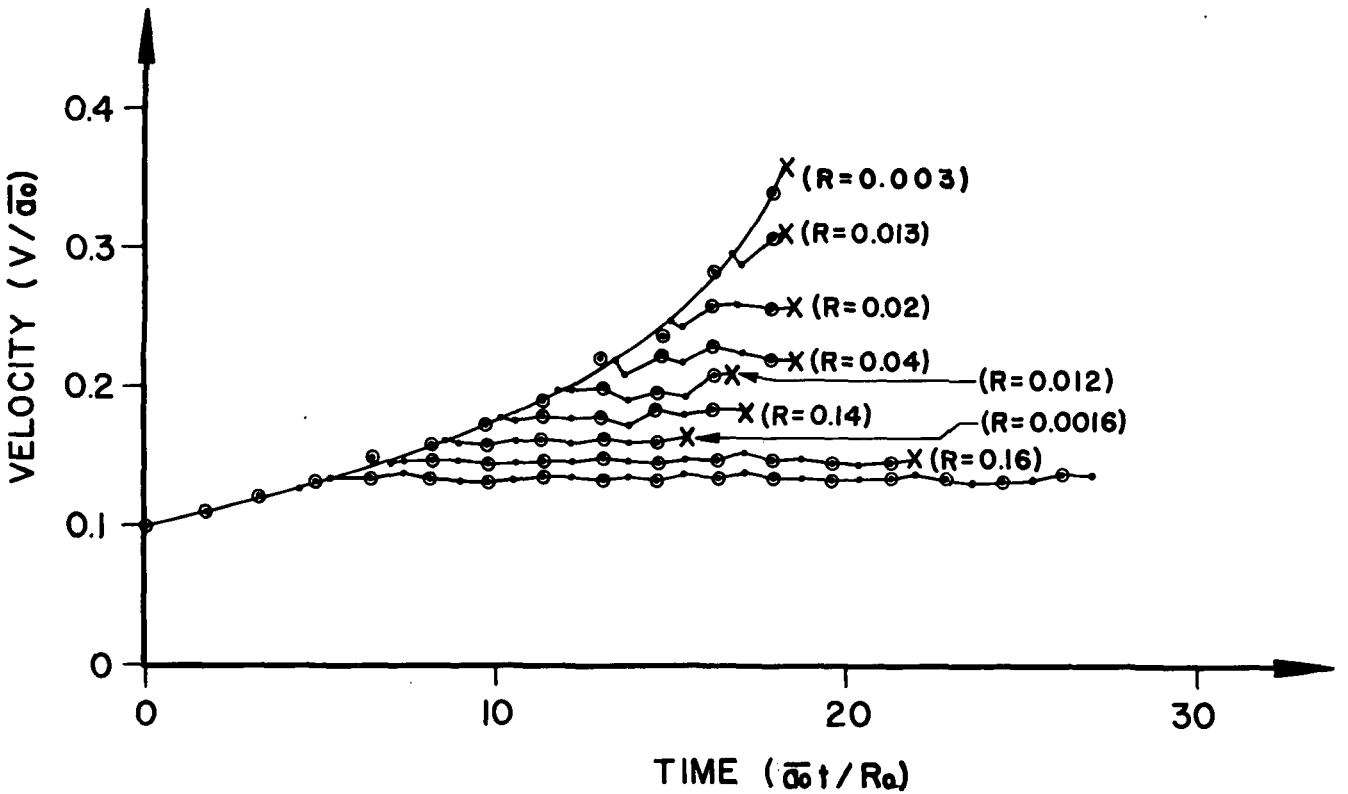

Figure 15. Wave oscillations after the amplifications with coefficient $\sigma = 0.05$ are stopped at various velocity magnitudes. R in bracket indicates non-dimensional radius, i.e. $R = r/R_o$.

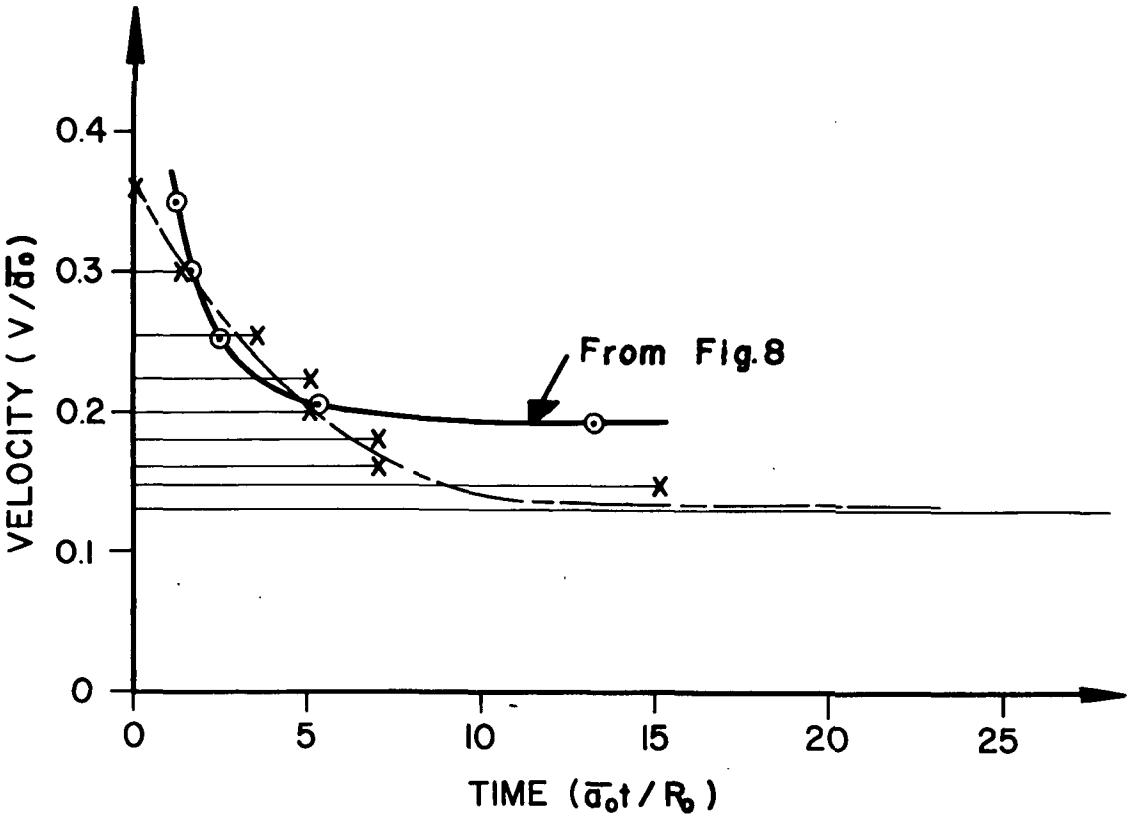

Figure 16. Estimate of the wave magnitude at which oscillation is permanent, for case (c). Ordinate (Time = 0 line) corresponds to the wave growth line with the amplification coefficient $\sigma = 0.05$ in Figure 15, i.e., time is measured from the time when the amplification is stopped. Circled points are transferred from Figure 8 of case (a), for comparison.

NASA-Langley, 1972 — 12 E-7114

NATIONAL AERONAUTICS AND SPACE ADMINISTRATION
WASHINGTON, D.C. 20546

OFFICIAL BUSINESS
PENALTY FOR PRIVATE USE $300

SPECIAL FOURTH-CLASS RATE
BOOK

POSTAGE AND FEES PAID
NATIONAL AERONAUTICS AND
SPACE ADMINISTRATION
451

U.S.MAIL

POSTMASTER : If Undeliverable (Section 158 Postal Manual) Do Not Return

"The aeronautical and space activities of the United States shall be conducted so as to contribute . . . to the expansion of human knowledge of phenomena in the atmosphere and space. The Administration shall provide for the widest practicable and appropriate dissemination of information concerning its activities and the results thereof."

—NATIONAL AERONAUTICS AND SPACE ACT OF 1958

NASA SCIENTIFIC AND TECHNICAL PUBLICATIONS

TECHNICAL REPORTS: Scientific and technical information considered important, complete, and a lasting contribution to existing knowledge.

TECHNICAL NOTES: Information less broad in scope but nevertheless of importance as a contribution to existing knowledge.

TECHNICAL MEMORANDUMS: Information receiving limited distribution because of preliminary data, security classification, or other reasons. Also includes conference proceedings with either limited or unlimited distribution.

CONTRACTOR REPORTS: Scientific and technical information generated under a NASA contract or grant and considered an important contribution to existing knowledge.

TECHNICAL TRANSLATIONS: Information published in a foreign language considered to merit NASA distribution in English.

SPECIAL PUBLICATIONS: Information derived from or of value to NASA activities. Publications include final reports of major projects, monographs, data compilations, handbooks, sourcebooks, and special bibliographies.

TECHNOLOGY UTILIZATION PUBLICATIONS: Information on technology used by NASA that may be of particular interest in commercial and other non-aerospace applications. Publications include Tech Briefs, Technology Utilization Reports and Technology Surveys.

Details on the availability of these publications may be obtained from:

SCIENTIFIC AND TECHNICAL INFORMATION OFFICE

NATIONAL AERONAUTICS AND SPACE ADMINISTRATION

Washington, D.C. 20546